Structural Engineering and Mechanics, *Vol. 89, No. 5 (2024) 479-489*
https://doi.org/10.12989/sem.2024.89.5.479

Numerical simulation of infill CACB wall cracking subjected to wind loads

Ruige Li*[1], Yu Gao[1], Hongjian Lin**[1], Mingfeng Huang[2], Chenghui Wang[3], Zhongzhi Hu[1] and Lingyi Jin[4]

[1]*School of Civil Engineering and Architecture, Taizhou University, Taizhou Jiaojiang, 318000, China*
[2]*School of Civil Engineering & Architecture, Zhejiang University, Hangzhou,310058, China*
[3]*Taizhou Institute of Planning and Design for Urban and Rural, Taizhou Jiaojiang, 318000, China*
[4]*Zhedong Engineering Investigation Institute, Taizhou Linhai, 317000, China*

(*Received November 6, 2023, Revised January 16, 2024, Accepted February 21, 2024*)

Abstract. The cracking mechanism in ceramsite aerated concrete block (CACB) infill walls were studied in low seismic fortification intensity coastal areas with frequent occurrence of typhoons. The inter-story drifts of an eight-story residential building under wind loads and a seismic fortification intensity of six degrees were analyzed by using the PKPM software. The maximum inter-story drift ratio of the structure in wind load was found to be comparable to that under the seismic fortification intensity of six degrees. However, when accounting for the large gust wind speed of typhoon, the maximum inter-story drift ratio was much larger than that obtained under reference wind load. In addition, the finite element models of RC frames were employed by displacement loading to simulate two scenarios with and without window hole in the CACB infill walls, respectively. The simulation results show no signs of cracking in both the infill walls with window hole and those without window for the inter-story drift caused by seismic loads and the reference wind load. However, both types of infill walls experienced structural creaking when assessing the gust wind pressure recorded from previous typhoon monitoring. It is concluded that an underestimate of wind loads may contribute substantially to the cracking of frame CACB infill walls in low seismic fortification intensity coastal areas. Consequently, it is imperative to adopt wind pressure values derived from gust wind speeds in the design of CACB infill walls within frame structures. Finally, the future research directions of avoiding cracks in CACB filled walls were proposed. They were the material performance improving and building structure optimizing.

Keywords: ceramsite aerated concrete block (CACB) infill wall; cracks; inter-story displacement; wind load

1. Introduction

According to the engineering investigation in the coastal area of Zhejiang province, China, there are many cracks in the ceramsite aerated concrete block (CACB) infill wall of reinforced concrete (RC) frame. The wall cracking is more serious in the coastal area than other areas, even if the materials, the design, and the construction methods are all the same, because of the frequently occurred wind actions in the southeast coastal areas of China due to specific geography and climate characteristics. The frequently occurred synoptic wind was thought to be the main cause of the wall cracking. Jiang *et al.* (2018), Li *et al.* (2022) have studied the wind pressure on structures in the coastal areas dominated by the typhoon climate. The RC frame structures have weak bending stiffness and cannot effectively resist the wind loads (Qi *et al.* 1991, Yan *et al.* 2010).

In China, typhoon makes landfall frequently and causes much damage (Huang *et al.*2020, Huang *et al.*2015). The southeast coast of China experiences more than three typhoons each year in average from 1951 to 2022, during which a total of 243 typhoons was recorded. The maximum wind speed near the center of Typhoon Lekima in August 2019 was over 60 m/s (Typhoon Webpage in National Meteorological Centre of China 2023), which corresponded to a wind pressure of about 2.34 kN/m^2. In the city, the wind load has a great influence on the buildings (Gu *et al.* 2023). The impact of extreme typhoon loads on the frame structure can result in significant inter-story displacement, which is an important consideration in the wind-resistant building design.

While earthquakes are often a main concern in building structural design, the damage caused by daily minor wind loads in low seismic intensity areas, particularly in coastal regions, is frequently overlooked. In a study conducted by Yuan *et al.* (2013), inter-story displacement and total displacement at the top of a 10-story frame structure were compared under a low seismic intensity of six degrees (with a design acceleration of 0.05 g) and a reference wind pressure of 0.45 kN/m^2. The analysis shows that the internal forces caused by wind loads were greater than that of seismic intensity of six degrees and controlled the design. During a landfall caused by typhoons and tropical storms, the wind load was suggested by Leng *et al.* (2013) to be far exceed 0.45 kN/m^2. Tong *et al.* (1982, 1985) found that the inter-story drift ratio of infill wall leading to cracking was much smaller than the plastic limit of inter-story drift ratio of RC frames. While the main structure subjected to wind

*Corresponding author, Associate Professor
E-mail: lrg@tzc.edu.cn
**Corresponding author, Senior Engineer
E-mail: linhj2011@tzc.edu.cn

ISSN: 1225-4568 (Print), 1598-6217 (Online)

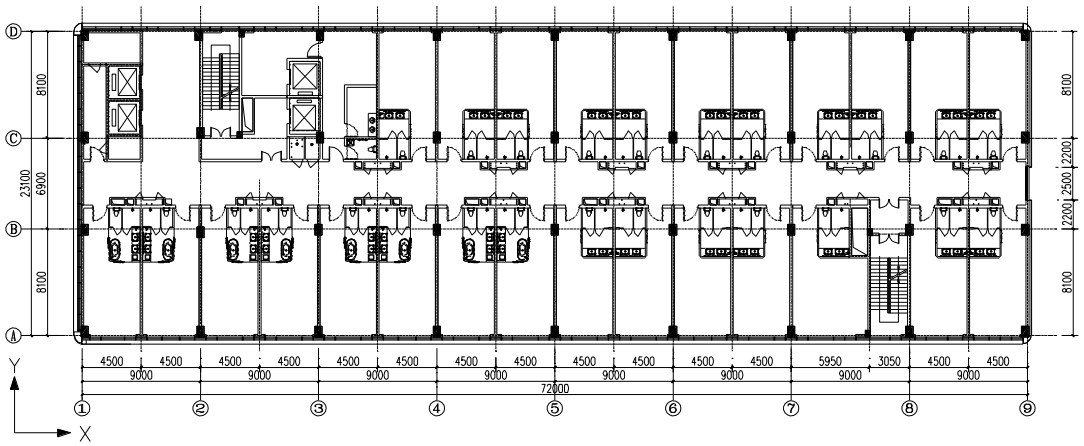

Fig. 1 Standard floor plan

loads remains elastic, the infill walls may be vulnerable to cracking due to their low strength and the wind-induced inter-story drift ratios. Moreover, the dynamic response of high-rise buildings to wind loads involves both turbulent fluctuating velocity and vortex shedding, resulting in structural vibration, fatigue, and torsional effects (Li *et al.* 2014, Jafari *et al.* 2020, Liu 2021). These complex loads can cause the infill wall with lower strength to crack due to the vibration and deformation of the main structure.

The literatures on cracks in infill walls are very limited. Most related studies focused the research on the mechanical characteristics of masonry infill walls in frame structures. The interaction between infill walls and frame members was studied through the proposed simplified infill wall model, and the influence of different wall design parameters on their mechanical performance was analyzed (Rui *et al.* 2020, Mohammed *et al.* 2022, Aslam *et al.* 2022). Studied on the mechanical properties of infilled frame structures and the effect of walls on the overall structure or adjacent column members could also be found (Flanagan *et al.* 1999, Arton *et al.* 2018, Mehmet *et al.* 2020). Mainstone (2016), Mazza (2019), Jiang *et al.* (2015) have proposed methods for estimating the stiffness and bearing capacity of infilled frame structures. It is worth noting that most existing research results highlight in-plane deformation as the primary cause of damage to masonry infill walls. Therefore, the in-plane mechanical properties and damage characteristics of masonry infill walls must be correctly understood to evaluate the seismic performance of infill walls and their influence on structures (Misir *et al.* 2016, Kamaris *et al.* 2016). On the concrete surface damage identification, Zhang *et al.* (2023) studied the method based on probabilistic deep learning of images that can detect the safety of concrete structures more accurately.

The research on cracks in CACB infill walls is crucial in assessing the applicability of buildings, particularly in coastal typhoon-prone areas. Infill wall cracks of a building may cause rain water leakage, which can seriously affect the functional use of housing. Thus, cracks in infill walls should not be overlooked, even though their impact on the safety of structures is limited.

Ceramsite is an environmental green material made from the waste mud obtained from foundation excavation.

Table 1 The floor height and component size

Floor	Floor height/m	Column $b \times h$ /mm×mm	Beam $b \times h$ /mm×mm
1	5.25	700×1000	350×1000
2	6.50	700×1000	350×1000
3	5.00	550 × 800	300×900
4	5.00	550 × 800	300×900
5	5.00	550× 600	300×900
6	4.40	550× 600	300×900
7	4.40	550× 600	300×900
8	3.40	500× 600	300×900

The ceramsite aerated concrete block (CACB) is a green building material made of ceramsite that has popularized continuously in the southeast coastal area of China as the frame filling wall (Lin *et al.* 2023) for a long time. However, the large number of wall cracks prevents the use of this material. The same trouble occurs with lightweight concrete block filled walls too. Therefore, it is important to study the causes of cracks in low-strength lightweight concrete block infill walls.

In this paper, a frame structure construction project located in Taizhou, Zhejiang province of China was analyzed by using PKPM to investigate the inter-story displacement under seismic and wind loads. Two finite element models of RC frame CACB infill wall were proposed, and a low cycle reciprocating loading test was performed. The finite simulation experiment aimed to investigate the relationship between infill wall crack development and inter-story drift ratio, as well as the correlation between structural stiffness and the crack development. Based on the comparison of PKPM and simulation model test results, the process and influencing factors of inclined cracks in CACB infill walls in the southeast coastal area of Zhejiang province were examined.

2. Building example

The construction project under consideration involves an eight-story frame structure residential building located in Taizhou, which is situated on the southeastern coast of Zhejiang province. The standard floor structure plan is

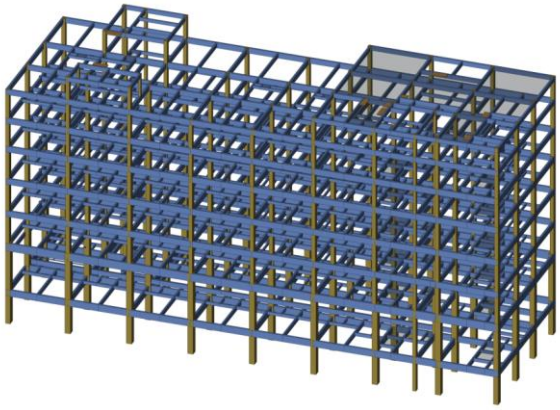

Fig. 2 Finite element model of the structure

listed in Fig. 1. The construction involved the use of C40 concrete for columns spanning the first to the third stories, C35 for the fourth story, and C30 for stories above the fifth level. The beams and slabs were reinforced with C30 concrete to ensure adequate strength. The columns and frame beams cross-section and the floor heights were shown in Table 1. The transverse and longitudinal frame beams had cross-sectional dimensions of 300 mm×900 mm, while other non-frame beams had dimensions of 250 mm×800 mm, 250 mm×600 mm, and 250 mm×450 mm, respectively. Fig. 2 depicts the structural finite element model used in the analysis.

3. Structural analysis of the building example

3.1 Wind loads

The coastal location of Taizhou city is susceptible to frequent landfall typhoons and strong winds. During the landfall of Typhoon Lekima in 2019, the 10-minute mean maximum wind speed recorded at the Sansuan meteorological observation station in Wenling, Taizhou was 48.2 m/s, while the maximum gust wind speed was 61.4 m/s. Additionally, two maximum wind velocities were recorded at the Dachen meteorological observation station in Jiaojiang District, Taizhou, reaching 42.4 m/s and 60.3 m/s, respectively. According to load code for the design of building structures (GB50009-2012 2012), extreme wind speed data were collected to determine the design wind speed and in turn to calculate the wind pressure as following

$$w = \frac{1}{2}\rho v^2 \tag{1}$$

where ρ is the density of the air, and v is the speed of wind. The ρ can be calculated by using the following formula suggested by GB50009-2012 (2012)

$$\rho = 0.00125\mathrm{e}^{-0.0001z} \tag{2}$$

where z is the altitude of concern.

In structural analysis, the local reference wind pressure as specified in the load code is typically used as the input wind load. For the design of building structures, the reference wind pressure is calculated based on the average wind speed over a 10-minute period, and the recurrence period of 50 years is considered according to the probability distribution of extreme value Type I (Jin *et al.* 2011). The construction project in Jiaojiang District, Taizhou has a reference wind pressure of 0.75 kN/m^2. However, during typhoons, gust wind brings a significant impact on the structure, often resulting in damage to both structural and non-structural components. At the Sansuan meteorological observation station, the peak wind pressure corresponding to the gust wind speed observed was 2.34 kN/m^2. Additionally, the wind pressure corresponding to the 10-minute mean maximum wind velocity was 1.44 kN/m^2. The wind speeds and pressures recorded in other areas of Taizhou are listed in Table 2.

In light of the significant impact of typhoons in this region, the structural analysis for the building example was conducted for five load combination cases.

In the analysis, the dead load is the self-weight of the structure, and the vertical live load is 2.0 kN/m^2 based on the *load code for the design of building structures* (GB50009-2012 2012*)*. The vertical live load of the upper roof is also 2.0 kN/m^2. The horizontal load is the earthquake action and wind load. In the analysis, there were five cases of horizontal loads listed in Table 3.

In Case 1, The seismic fortification intensity of six degree was from the design code (GB18306-2015),

Table 2 Wind speed measurements over Taizhou during Typhoon Lekima landfall in 2019

No.	District	Weather station	Altitude /m	Average maximum wind speed of 10 min /(m/s)	Maximum wind speed of gusts/(m/s)	Wind pressure corresponding to average maximum wind speed of 10 min/(kN/m^2)	Wind pressure corresponding to maximum wind speed of gusts/(kN/m^2)
1	Wenling	Sansuan	80	48.2	61.4	1.44	2.34
2	Jiaojiang	Shangdachen	56	42.4	60.3	1.12	2.26
3	Wenling	Shitang	26	41.1	55.5	1.05	1.92
4	Wenling	Wenqiao	27	28.7	51.8	0.51	1.67
5	Wenling	Jiudongmen	55	36.7	50.9	0.84	1.61
6	Jiaojiang	Taizhouwan bridge	21	38.4	46.9	0.92	1.37
7	Wenling	Chengbei	35	32.0	46.3	0.64	1.34
8	Wenling	Functional area of grain	7	28.4	43.2	0.50	1.17
9	Wenling	Practice base	10	29.1	43.0	0.53	1.15
10	Jiaojiang	Dachen	66	30.8	45.4	0.59	1.27

Table 3 Five cases of horizontal loads in project analysis

Case	Earthquake action	Wind loads/kN/m^2
Case 1	Seismic intensity of six degree	0
Case 2	0	0.75
Case 3	0	1.27
Case 4	0	1.67
Case 5	0	1.92

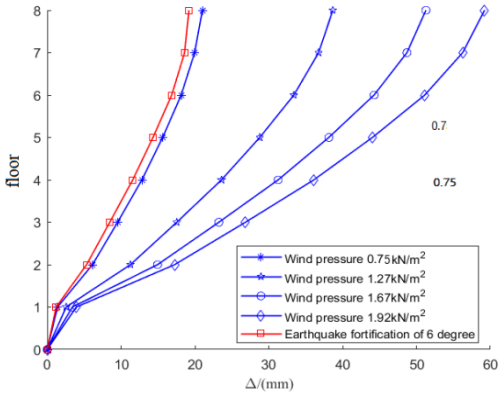

Fig. 3 The maximum y-directional displacements of the building example

In Case 2, the wind load is the reference wind pressure in this area from the load code (GB50009-2012, 2012).

In Case 3, the wind pressure value is corresponding to the wind speed of the Dachen gust in Jiaojiang.

In Case 4, the wind pressure value is corresponding to the wind speed of the wind gust at Wenqiao, Wenling.

In Case 5, the wind pressure value is corresponding to the wind speed of the gust in Shitang, Wenling.

3.2 Finite element software and analysis assumptions

A finite element method software PKPM for building structures developed in China is utilized for carrying out structural analysis of the building example (Wu 2013, Mi *et al.* 2022). The 2D beam element is used in the finite element method to model the beam, column, and supporting members of the building structure (Wan 2013). In this building example, the floor slab's stiffness is assumed to be infinite in the plane, and the resistance and stiffness of the infill wall are not considered when analyzing the internal forces and lateral displacement of the structure. The damping ratio of the structure is set to 5% when computing the internal forces under earthquake and wind loads (Li 1997, Wang 2016). The surface roughness is categorized as class B according to the load code (GB50009-2012 2012).

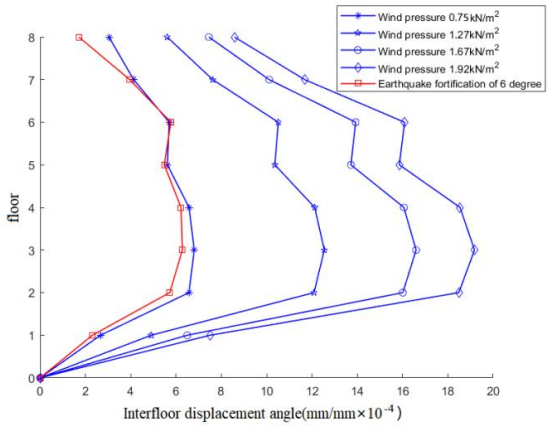

Fig. 4 The maximum y-directional inter-story drift ratio profiles of the building example

3.3 Structural analysis results

The inter-story displacements and inter-story drift ratios under both earthquake and wind loads are presented in Table 4. Fig. 3 presents the displacement responses of each story under varying wind pressure or earthquake excitations. Inter-story drift ratio profiles of the multi-story building are shown in Fig. 4. In Case 1, the maximum inter-story drift is observed at the intersection of the D-axis and 9-axis of the third floor, considering a seismic fortification intensity of six degrees. The corresponding maximum inter-story drift ratio is 1/1634. Additionally, when a Y-direction wind load of 0.75 kN/m^2 is applied, the maximum displacement occurs at the same location, with a maximum inter-story drift ratio of 1/1470. In Case 2, under the action of Y-direction wind load, the maximum inter-story displacement is also observed at the intersection of the D-axis and 9-axis of the third floor, with an inter-story drift ratio of 1/797. Similarly, in Case 3 and Case 4, the maximum inter-story displacements and drift ratios are

Table 4 Maximum inter-story displacements and inter-story drift ratio of the building example

Floor	Wind load of 0.75 kN/m^2		Wind load of 1.27kN/m^2		Wind load of 1.67kN/m^2		Wind load of 1.92kN/m^2		Seismic intensity of six degree	
	Δ*/mm	θ/×10^{-4}	Δ/mm	θ/×10^{-4}	Δ/mm	θ/×10^{-4}	Δ/mm	θ/×10^{-4}	Δ/mm	θ/×10^{-4}
1	1.4	2.67	2.57	4.90	3.41	6.50	3.94	7.50	1.21	2.30
2	4.73	6.57	8.7	12.09	11.53	16.01	13.31	18.49	4.12	5.72
3	3.4	6.80	6.27	12.55	8.3	16.60	9.59	19.18	3.14	6.28
4	3.29	6.57	6.06	12.12	8.03	16.06	9.27	18.54	3.11	6.22
5	2.81	5.62	5.18	10.36	6.86	13.72	7.93	15.86	2.74	5.48
6	2.51	5.70	4.62	10.52	6.13	13.93	7.08	16.09	2.54	5.77
7	1.82	4.13	3.35	7.62	4.45	10.11	5.14	11.68	1.74	3.95
8	1.05	3.04	1.93	5.61	2.57	7.45	2.96	8.58	0.59	1.71

*Δ: The maximum inter-story displacements; θ: Inter-story drift ratio.

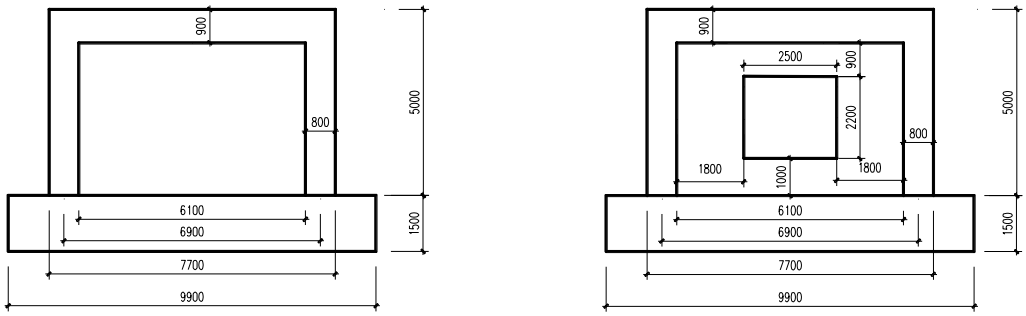

(a) RC frame infill wall without window (b) RC frame infill wall with window

Fig. 5 Details of the finite element model

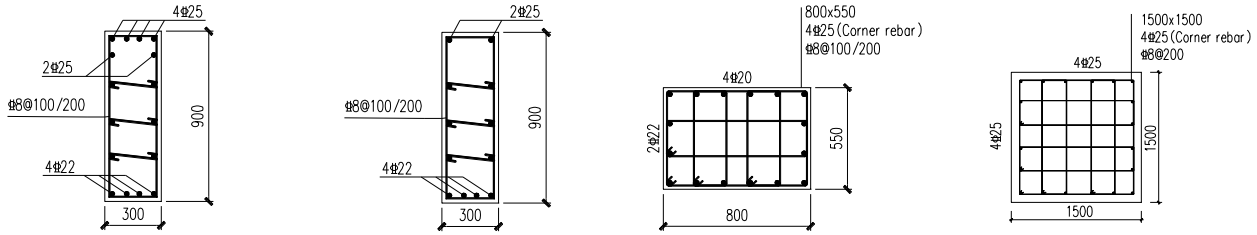

(a) The end of beam (b) The mid-span of beam (c) The column section (d) Frame base section

Fig. 6 Section dimension and reinforcement diagram of frame model

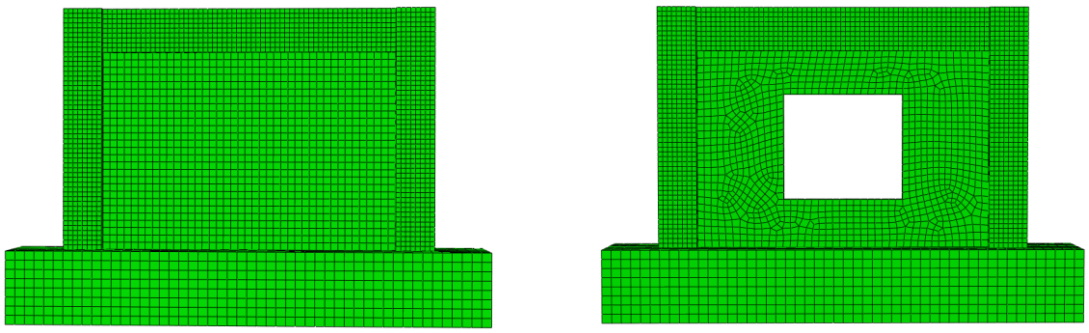

(a) RC frame infill wall without window (b) RC frame infill wall with window

Fig. 7 Element division diagram of finite element model

observed at the same location. Specifically, in Case 3, the maximum inter-story drift ratio is 1/602, while in Case 4, the maximum inter-story drift ratio is 1/521.

4. Numerical simulations of the infill wall

Two finite element model specimens of ABAQUSE were designed to study the relationship of the frame inter-story displacement and the infill wall cracks under horizontal load. The finite element specimen of the windowless corresponded to the wall between the B and C axis of the 1st axis in the third floor. And the specimen with the window hole is the wall between the B and C axes of the 9th axes in the third floor as shown in Fig. 1. The finite element model tests were carried out by quasi-static horizontal and vertical loads.

4.1 Infill wall model design

The finite element model was established to adhere to the design principle of strong column and weak beam, while also meeting the necessary structural requirements. The dimensions and reinforcement of the specimen can be seen in Figs. 5-8. The reinforced bars for both the beam and column have a strength grade of HRB400. The stirrups are present throughout the entire length of the beam and column. With beam end 1.35 m and column end 0.9 m, stirrup spacing is 100 mm, and other spacing is 200 mm. The frame concrete has a design strength grade of C40, and

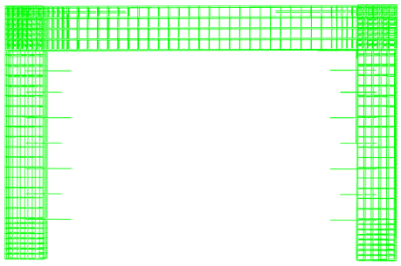

Fig. 8 The finite element model of tie bead and reinforced skeleton arrangement

the frame column has a design axial compression ratio of n=0.3 with an axial force of 2521.2 kN. The infill walls are constructed using CACB special masonry mortar. To ensure stability, seven rows of tie bars were added based on the number of layers of blocks, with the first, third, fifth, and seventh layers having a tie bar length of 900 mm and the second, fourth and sixth layers having a length of 700 mm.

4.2 Constitutive model of materials

Reference to *Code for Design of Concrete Structure* (GB 50010-2010 2015) and material test results, the stress-strain constitutive of steel bars is

$$\sigma_s = \begin{cases} E_s & \varepsilon_s \le \varepsilon_y \\ f_{y,r} & \varepsilon_y < \varepsilon_s \le \varepsilon_{uy} \\ f_{y,r} + k(\varepsilon_s - \varepsilon_{uy}) & \varepsilon_{uy} < \varepsilon_s \le \varepsilon_u \\ 0 & \varepsilon_s > \varepsilon_u \end{cases} \tag{3}$$

$$\varepsilon_y = \frac{f_{y,r}}{E_s} \tag{4}$$

where E_s was the elastic modulus of a bar, σ_s and ε_s were the stress and the strain of the bar, respectively. $f_{y,r}$ was the yield strength of the steel bar; $f_{st,r}$ was the ultimate strength; ε_y is the yield strain of the bar corresponding to $f_{y,r}$, ε_{uy} was the hardening starting strain of steel bar, ε_u is the peak strain corresponding to $f_{st,r}$, and k was the slope of the hardened section of the steel bar as shown in equation (5).

$$k = (f_{st,r} - f_{y,r})/(\varepsilon_u - \varepsilon_{uy}) \tag{5}$$

Reference to Code for Design of Concrete Structure (GB 50010-2010 2015), the stress-strain constitutive equation of steel bar under repeated loading is as follows

$$\sigma_s = E_s(\varepsilon_s - \varepsilon_a) - (\frac{\varepsilon_s - \varepsilon_a}{\varepsilon_b - \varepsilon_a})^p [E_s(\varepsilon_b - \varepsilon_a) - \sigma_b] \tag{6}$$

$$p = \frac{(E_s - k)(\varepsilon_b - \varepsilon_a)}{E_s(\varepsilon_b - \varepsilon_a) - \sigma_b} \tag{7}$$

where ε_a is the strain corresponding to the starting point of the reloading path, where ε_b and σ_b are the stress and strain corresponding to the end point of the reloading path, if the steel bar has not yielded in the direction of loading, the values were the strain and stress at the initial yield point of the reinforcement, if the bar has yielded in the loading direction, the value was the historical maximum strain of the bar in that direction.

The stress-strain curve of CACB under uniaxial tension was determined according to the following formula (GB 50010-2010 2015)

$$\sigma = (1 - d_t)E_c\varepsilon \tag{8}$$

$$d_t = \begin{cases} 1 - \rho_t[1.2 - 0.2x^5] & x \le 1 \\ 1 - \frac{\rho_t}{\alpha_t(x-1)^{1.7} + x} & x > 1 \end{cases} \tag{9}$$

$$x = \frac{\varepsilon}{\varepsilon_{t,r}} \tag{10}$$

$$\rho_t = \frac{f_{t,r}}{E_c\varepsilon_{t,r}} \tag{11}$$

Table 5 Finite element simulation results

θ (×10^{-4})	The frame-filled wall without window holes		The frame-filled wall with window holes	
	Corresponding load	Horizontal force (kN)	Corresponding load	Horizontal force (kN)
6.288	*S6	516.58	*S6	338.20
6.768	0.75 kN/m^2	624.26	0.75 kN/m^2	385.15
12.462	1.27 kN/m^2	1322.80	1.27 kN/m^2	1053.23
16.730	1.67 kN/m^2	1037.96	1.67 kN/m^2	1250.27
19.150	1.92 kN/m^2	807.37	1.92 kN/m^2	778.68

*S6: Seismic loads of six degree level; θ: Inter-story drift ratio.

where d_t was the damage evolution parameter of ceramsite concrete under uniaxial tension; α_t was a parameter value of 0.25 for the stress-strain curve section of ceramsite concrete under uniaxial tension, $\varepsilon_{t,r}$ was the representative value of the uniaxial tensile strength of ceramsite concrete, and the value is 0.605 N/mm^2; $\varepsilon_{t,r}$ was the peak tensile strain corresponding to the representative value $\varepsilon_{t,r}$ of uniaxial tensile strength, which was 1.00×10^{-3}.

The stress-strain curve for the uniaxial compression of aerated ceramsite concrete was as follows

$$\sigma = (1 - d_c)E_c\varepsilon \tag{12}$$

$$d_c = \begin{cases} 1 - \frac{\rho_c n}{n - 1 + x^n} & x \le 1 \\ 1 - \frac{\rho_c}{\alpha_c(x-1)^2 + x} & x > 1 \end{cases} \tag{13}$$

$$\rho_c = \frac{f_{c,r}}{E_c\varepsilon_{c,r}} \tag{14}$$

$$n = \frac{E_c\varepsilon_{c,r}}{E_c\varepsilon_{c,r} - f\varepsilon_{c,r}} \tag{15}$$

$$x = \frac{\varepsilon}{\varepsilon_{c,r}} \tag{16}$$

where α_c was the parameter value of the descending stress-strain curve of ceramsite concrete under uniaxial compression, and which was 6.0; $f_{c,r}$ was the representative value of the uniaxial compressive strength of ceramsite concrete, and the value is 5.035 N/mm^2; $\varepsilon_{c,r}$ was the peak compressive strain corresponding to the representative value $f_{c,r}$ of uniaxial compressive strength, which was 0.00303.

4.3 The loading process

Initially, a vertical load of 702 kN is applied to each column, divided into four levels, with each level increasing by 351 kN. Once the vertical load reaches the target value, it is maintained at a constant level, and a horizontal load is then applied. The horizontal load starts at 40 kN and increases by 10 kN for each cycle until it reaches yield.

4.4 Simulation results analysis

According to the results of finite element simulation, the horizontal force and the analysis of the inter-story drift ratio corresponding to seismic loads of six-degree level and wind loads of 0.75, 1.27, 1.67, 1.92 kN/m^2 are listed in Table 5.

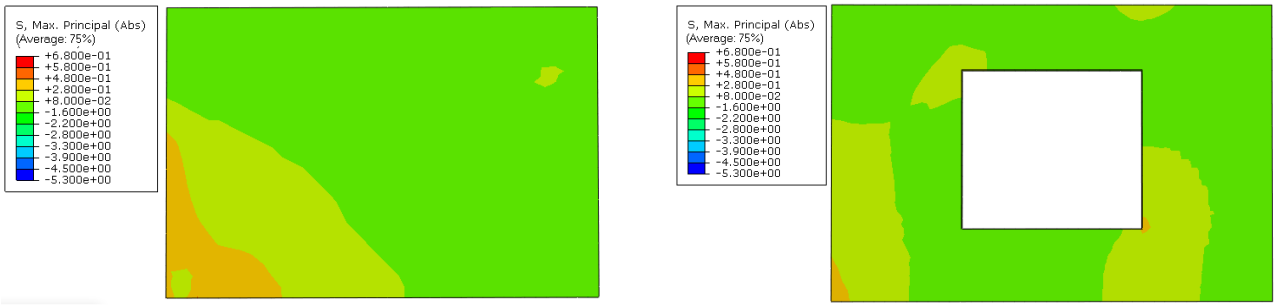

(a) CACB infill wall without window (b) CACB infill wall with window

Fig. 9 The CACB wall stress corresponds to the inter-story drift ratio of seismic load of 6-degree fortification

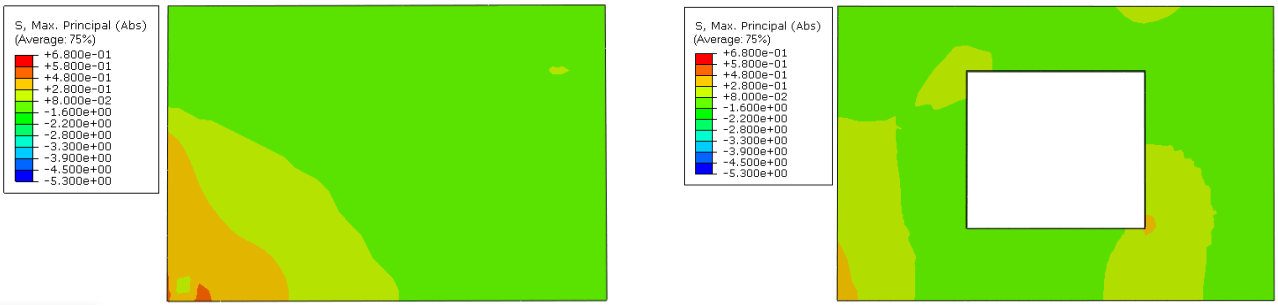

(a) CACB infill wall without window (b) CACB infill wall with window

Fig.10 The CACB wall stress corresponds to the inter-story drift ratio of wind load 0.75 kN/m^2

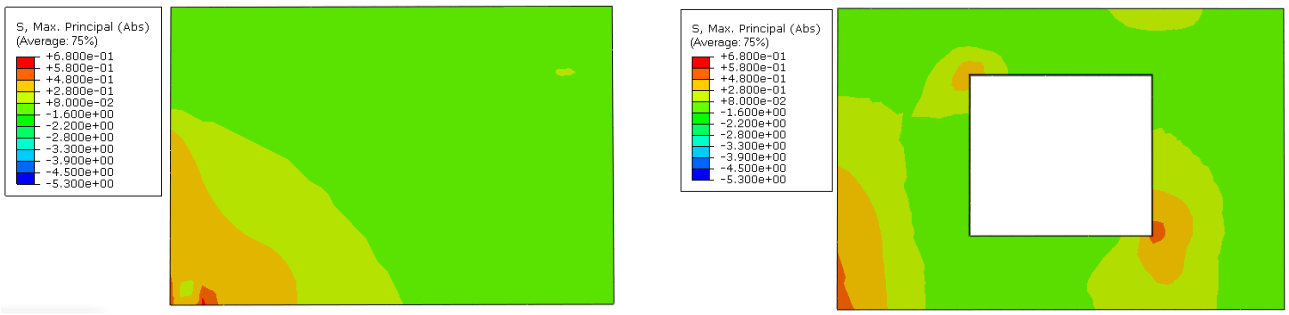

(a) CACB infill wall without window (b) CACB infill wall with window

Fig. 11 The CACB wall stress corresponds to the inter-story drift ratio of wind load 1.27 kN/m^2

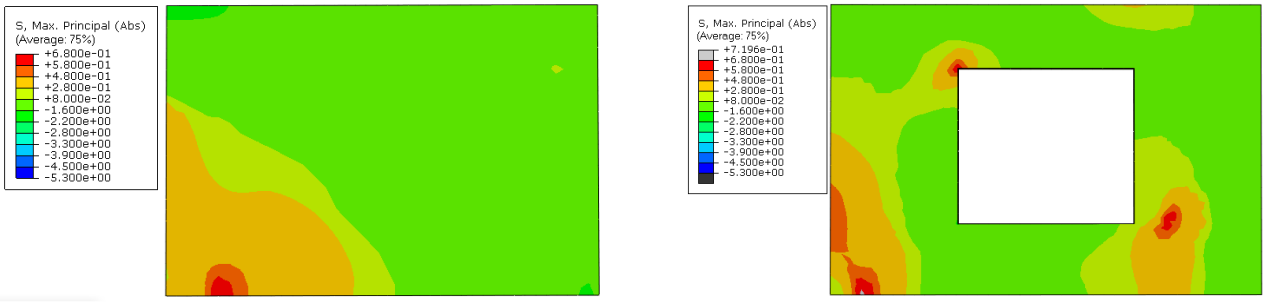

(a) CACB infill wall without window (b) CACB infill wall with window

Fig. 12 The CACB wall stress corresponds to the inter-story drift ratio of wind load 1.67 kN/m^2

The stress cloud of the finite element model of CACB filled wall under various loads were shown in Fig. 9-Fig. 13. The PE (plastic strain component) diagrams were shown in Fig. 14-Fig. 17.

It can be seen from the simulation stress and plastic strain component nephogram that when the inter-story drift ratio simulated by ABAQUS software close that caused by seismic load of six degree fortification and the wind load of 0.75 kN/m^2, the infill wall did not crack as shown in Fig. 9, Fig. 10, Fig. 14 and Fig.15.

When the inter-story drift ratio close that caused by wind load of 1.27 kN/m^2, there was a small area cracking in

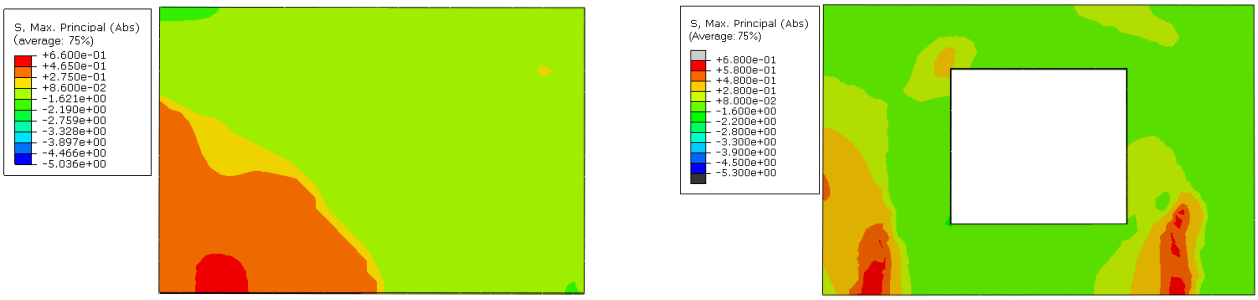

(a) CACB infill wall without window (b) CACB infill wall with window

Fig. 13 The CACB wall stress corresponds to the inter-story drift ratio of wind load 1.92 kN/m^2

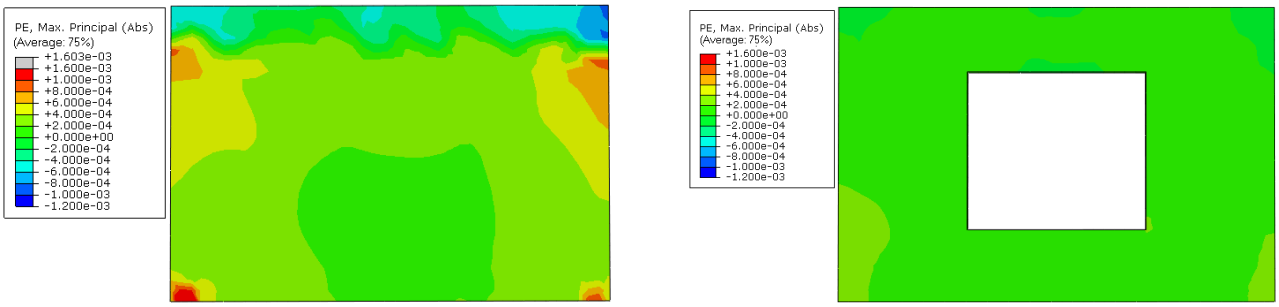

(a) CACB infill wall without window (b) CACB infill wall with window

Fig. 14 The CACB wall PE corresponds to the inter-story drift ratio of seismic load of 6-degree fortification

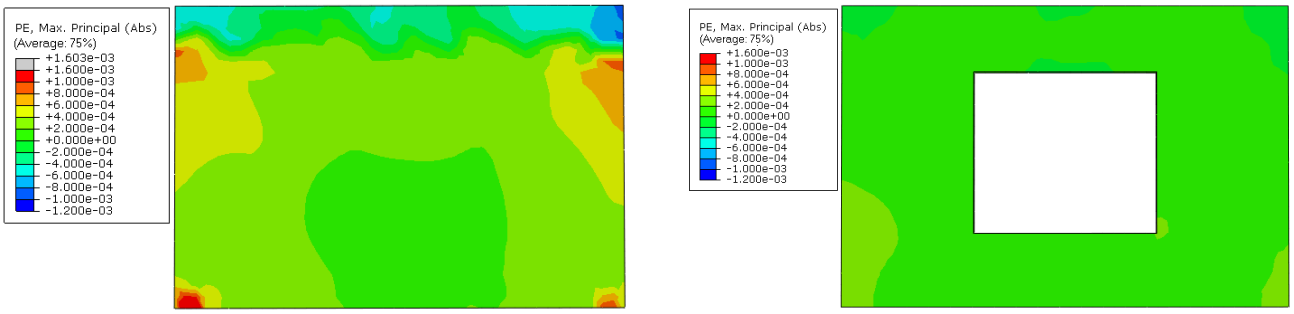

(a) CACB infill wall without window (b) CACB infill wall with window

Fig. 15 The CACB wall PE corresponds to the inter-story drift ratio of wind load 0.75 kN/m^2

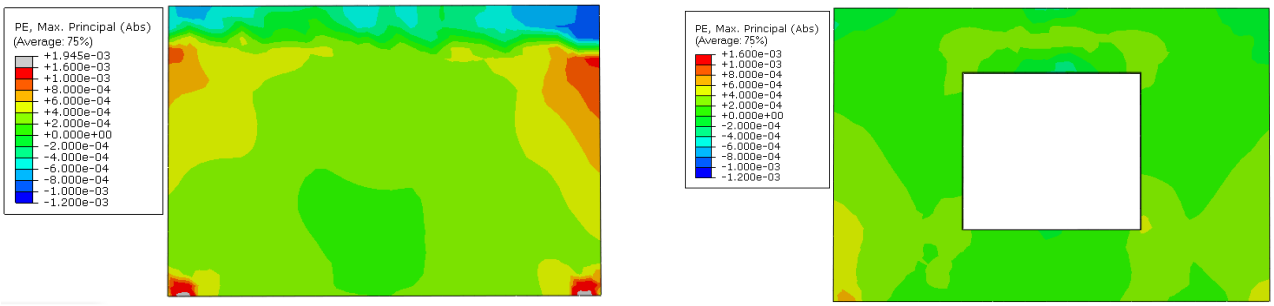

(a) CACB infill wall without window (b) CACB infill wall with window

Fig. 16 The CACB wall PE corresponds to the inter-story drift ratio of wind load 1.27 kN/m^2

the bottom corner of the infill wall without window. But the filling wall with window didn't crack as shown in Fig. 11, and Fig. 16.

When the inter-story drift ratio close that caused by wind load of 1.67 kN/m^2, the crack area was larger than that in 1.27 kN/m^2 in the bottom corner of the infill wall without window, and the wall with window began cracking in two bottom corners of the window hole and two bottom corners of the wall, as shown in Fig. 12 and Fig. 17.

When the inter-story drift ratio close that caused by wind load 1.92 kN/m^2, the cracking areas in the corner of the windowless infill wall increased slightly, but in the wall

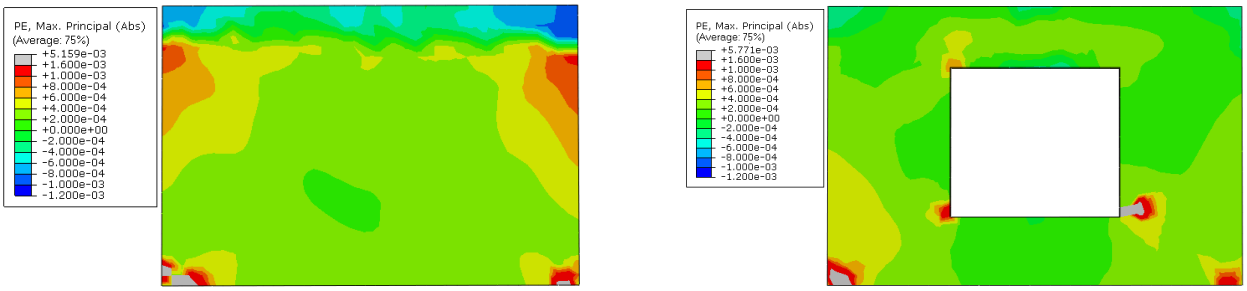

(a) CACB infill wall without window (b) CACB infill wall with window

Fig. 17 The CACB wall PE corresponds to the inter-story drift ratio of wind load 1.67 kN/m^2

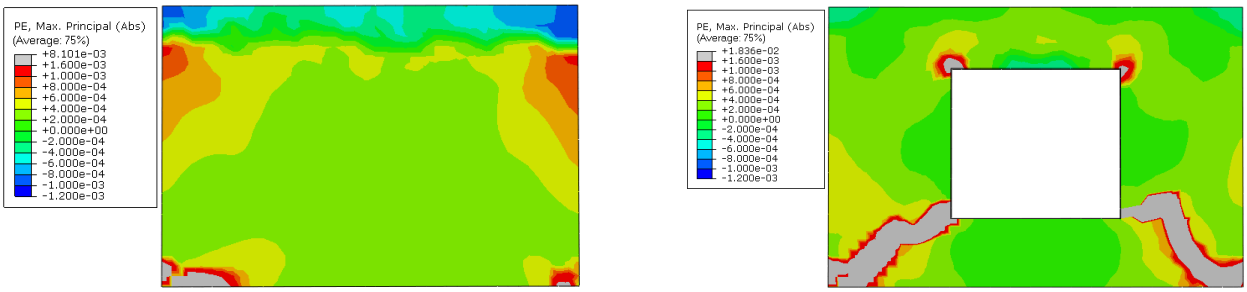

(a) CACB infill wall without window (b) CACB infill wall with window

Fig. 18 The CACB wall PE corresponds to the inter-story drift ratio of wind load 1.92 kN/m^2

with window, the crack areas increased largely in the low corners of the window and extends to the corner of the wall. The up corners of the window cracked too, as shown in Fig. 13 and Fig. 18.

4.5 Validation of numerically simulated response of infilled-frame interaction

According to the experimental results of Li *et al.* (2022), when the horizontal force is 90 kN, the inter-story drift angle reaches 1/1025 (that is, 9.756×10^{-4}), and the CACB infill wall appears cracks. Compared with the results of numerical simulation in this paper, the inter-story drift angle corresponds to the reference wind pressure between 0.75 (the corresponding drift angle is 6.768×10^{-4}) and 1.67 kN/m^2 (the corresponding drift angle is 12.462×10^{-4}). As can be seen from Figs. 10(a) and 11(a), when the wind load is 0.75 kN/m^2, the wall stress does not reach the ultimate, indicating that the wall has not cracked. When the wind load reaches 1.27 kN/m^2, the tensile stress in some areas of the lower left corner of the wall has reached the ultimate value of 0.605 N/mm^2, which indicates that the wall has begun to crack. The same conclusion can be observed in PE cloud Figs. 15(a) and 16(a). When the wind load is 0.75 kN/m^2, the wall stress does not reach the ultimate, indicating that the wall has not cracked. When the wind load reaches 1.27 kN/m^2, the tensile strain in the lower left corner of the wall exceeds the ultimate of 0.0010 in CACB, which proves that the wall has cracks at that time. It shows that the numerical simulation results of this paper agree with the experimental results of Li *et al.* (2022).

4.6 The problem of reference wind pressure in the design specification

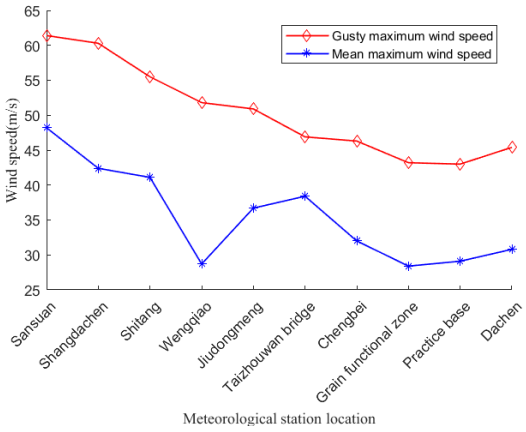

Fig. 19 Extreme wind speeds at stations of Taizhou in typhoon Lekima 2019

In coastal areas, the wind load on building structures is due to the actual wind pressure which is much higher than the reference value specified in the load code for structural design. Typically, the input reference wind load value in structural analysis is based on the average maximum wind speed of 10 minutes. However, during a typhoon, the average maximum speed of a gust in 3 min is often much higher than that of 10 as shown in Table 2. The average maximum wind speeds in 10 min and gusty average maximum speeds in 3 min at several meteorological stations during the landfall of Typhoon Lekima 2019 were shown in Fig. 19. Consequently, gusts have a considerable pressure on the structure and often cause damage to non-structural components. Therefore, the reference wind load value of 10 minutes average maximum wind speed in the design code is inadequate for façade design of buildings in typhoon-prone regions.

Compared the simulation results of ABAQUSE and PKPM, it can be seen that the CACB infill wall of the frame building will crack when the wind speed exceeds 33.5 m/s (corresponding to a wind load of 0.75 kN/m^2). According to typhoon monitoring data in Taizhou, gust wind speeds far exceeded 33.5 m/s and even reached over 60 m/s during typhoon landfall, which was far beyond the 6 degrees of seismic fortification when considering earthquake loads. For instance, during Typhoon Lekima in 2019, the actual maximum gust wind speed in Shitang, Wenling was recorded to be 61.4 m/s, which corresponded to the wind pressure of 2.34 kN/m^2. This value had largely exceeded the reference wind pressure. Therefore, serious cracklings of the CACB infill wall become inevitable. It can be concluded that the wind loads derived from the current load code for design of building structures, i.e., GB50009-2012, are inadequate to mitigate the potential hazards of CACB infill wall cracking.

5. Conclusions

Based on the results of PKPM analysis and the numerical simulation with ABAQUS, the primary cause of cracking in RC frame CACB infill walls is investigated in terms of wind-induced performance-based design.

- The southeast coastal area of Zhejiang province has low seismic fortification intensity, and wind load is the primary horizontal load. The current Chinese load code specifies a reference wind pressure that is calculated based on the mean maximum wind speed of 10 minutes for a given return period may be adequate for the wind-resistant design of main framework structure, but poses a risk of infill wall cracking due to underestimation of gust wind speed during typhoon events.
- The deformation ability of infill wall with window is better than that of windowless infill wall. When the wind load is small, the stress in the wall with window is much smaller than that in the wall without windows. When the applied inter-story drift ratio is close to that caused by gust wind, a lot of cracks will appear in both infill walls with window and without window.
- The infill wall of CACB block will inevitably crack with the current approach of primary structure engineering design and construction. Avoiding inclined cracks in infill walls by controlling inter-story drift will result in substantial waste in designing the main frame structure.
- To prevent crack in CACB infill wall caused by wind loads, two aspects are proposed in the future work. On the one hand, new materials additives, fiber for instance, maybe added into CACB to improve the deformation ability and strength, and thus the cracks of the infill wall are reduced. On the other hand, new flexible connection modes of frame and infill wall may also reduce the stress and strain of the infill wall and thus the cracks. In structure, given a certain gap between the infill wall and the frame, the deformation would reduce when the frame has a large horizontal displacement. Of course, we can also solve this problem from both materials and structure design points of view.

Acknowledgments

This research was funded by Zhejiang Provincial Natural Science Foundation with grant number LGG20E080006 and the National Natural Science Foundation of China Youth Science Foundation Project with grant number 52009087/E0903. We appreciate the Taizhou Meteorological Bureau for providing the wind speed, wind direction and other meteorological data.

References

Bouarroudj, M.A. and Boudaoud, Z. (2022), "Numerical investigation of predicting the in-plane behavior of infilled frame with single diagonal strut models", *Struct. Eng. Mech.*, **81**(2), 131-146. https://doi.org/10.12989/sem.2022.81.2.131.

Dautaj, A.D., Kadiri, Q. and Kabashi, N. (2018), "Experimental study on the contribution of masonry infill in the behavior of RC frame under seismic loading", *Eng. Struct.*, **165**, 27-37. https://doi.org/10.1016/j.engstruct.2018.03.013.

Flanagan, R.D. and Bennett, R.M. (1999), "Bidirectional behavior of structural clay tile infilled frames", *J. Struct. Eng.*, **125**(3), 236-244. https://doi.org/10.1061/(ASCE)0733-9445(1999)125:3(236).

GB18306-2015 (2015), General Administration of Quality Supervision Inspection and Quarantine of China, Seismic Ground Motion Parameters Donation Map of China, China Standard Press, Beijing. (in Chinese)

GB50009-2012 (2012), Load Code for the Design of Building Structure, Ministry of Housing and Urban-Rural Development of the Peoples Republic of China, China Construction Industry Press, Beijing. (in Chinese)

GB50010-2010 (2015), Code for Design of Concrete Structure, Ministry of Housing and Urban-Rural Development of the People Republic of China, China Construction Industry Press, Beijing. (in Chinese)

Gu, D., Kareem, A., Lu, X. and Cheng, Q. (2023), "A computational framework for the simulation of wind effects on buildings in a cityscape", *J. Wind Eng. Ind. Aerod.*, **234**(1), 105347. https://doi.org/10.1016/j.jweia.2023.105347.

Huang M.F., Sun J.P., Wang Y.F., *et al.* (2020), "Multi-scale simulation of typhoon wind fields by coupling of weather research and forcasting model and large-eddy simulation", *J. Build. Struct.*, **41**(2), 63-70. https://doi.org/10.14006/j.jzjgxb.2018.0735.

Huang, M.F., Li, Q., Chan, C.M., Lou, W.J., Kwok, K.C. and Li, G. (2015), "Performance-based design optimization of tall concrete framed structures subject to wind excitations", *J. Wind Eng. Ind. Aerod.*, **139**, 70-81. https://doi.org/10.1016/j.jweia.2015.01.005.

Jafari, M. and Alipour, A. (2021), "Methodologies to mitigate wind-induced vibration of tall buildings: A state-of-the-art review", *J. Build. Eng.*, **33**, 101582. https://doi.org/10.1016/j.jobe.2020.101582.

Jiang, H., Liu, X. and Mao, J. (2015), "Full-scale experimental study on masonry infilled RC moment-resisting frames under cyclic loads", *Eng. Struct.*, **91**, 70-84. https://doi.org/10.1016/j.engstruct.2015.02.008.

Jiang, R., Jiang, L., Hu, Y., Ye, J. and Zhou, L. (2020), "A simplified method for estimating the fundamental period of masonry infilled reinforced concrete frames", *Struct. Eng. Mech.*, **74**(6), 821-832. https://doi.org/10.12989/sem.2020.74.6.821.

Jiang, X.Q., Li, R.G., Li, Q., *et al.* (2018), "Research on the method of basic wind pressure in coastal areas with insufficient meteorological observation data: Taking Taizhou as an example", *J. Taizhou Univ.*, **40**(6), 50-57+63. https://doi.org/10.13853/j.cnki.issn.1672-3708.2018.06.009.

Jin, X.Y., Chen, K., Tang, Y., *et al.* (2011), "New progress of research and application of wind engineering for buildings", *Build. Struct.*, **41**(11), 111-117. https://doi.org/10.19701/j.jzjg.2011.11.023.

Kamaris, G.S., Skalomenos, K.A., Hatzigeorgiou, G.D. and Beskos, D.E. (2016), "Seismic damage estimation of in-plane regular steel/concrete composite moment resisting frames", *Eng. Struct.*, **115**, 67-77. https://doi.org/10.1016/j.engstruct.2016.01.053.

Komur, M.A., Kara, M.E. and Deneme, I.O. (2020), "Infill wall effects on the dynamic characteristics of RC frame systems via operational modal analysis", *Struct. Eng. Mech.*, **74**(1), 121-128. https://doi.org/10.12989/sem.2020.74.1.121.

Leng, Y., Fan, C. and Tang, H. (2013), "A comparison and analysis on response between wind and earthquake action on tall buildings", *J. Yangzhou Univ. (Nat. Sci. Ed.)*, **16**(3), 65-69. https://doi.org/10.19411/j.1007-824x.2013.03.016.

Li, L., Zhang, J.W. and Li, Q.S. (2014), "Experimental investigation of characteristics of torsional wind loads on rectangular tall buildings", *Struct. Eng. Mech.*, **49**(1), 129-145. http://doi.org/10.12989/sem.2014.49.1.129.

Li, R., Wang, Y., Lin, H., Du, H., Wang, C., Chen, X. and Huang, M. (2022), "A mesoscale CFD simulation study of basic wind pressure in complex terrain-a case study of Taizhou city", *Appl. Sci*., **12**(20), 10481. https://doi.org/10.3390/app122010481.

Li, Y. and Mau, S.T. (1997), "Learning from recorded earthquake motion of buildings", *J. Struct. Eng.*, **123**(1), 62-69. https://doi.org/10.1061/(ASCE)0733-9445(1997)123:1(62).

Lin, H., Zhu, B., Yuan, J., He, H., Li, R., Yu, J., ... & Xu, W. (2023), "Study on the impact of HTPP fibers on the mechanical properties of ceramsite concrete", *Case Stud. Constr. Mater.*, **19**, e02471. https://doi.org/10.1016/j.cscm.2023.e02471.

Liu, Y., Li, H.N., Li, C. and Dong, T.Z. (2021), "Lifetime seismic performance assessment of high-rise steel-concrete composite frame with buckling-restrained braces under wind-induced fatigue", *Struct. Eng. Mech.*, **77**(2), 197-215. https://doi.org/10.12989/sem.2021.77.2.197.

Mainstone, R. (1971), "On the stiffnesses and strengths of infilled frames", *Proc. Inst. Civil Eng*., **49(2)**, 230. https://doi.org/10.1680/iicep.1971.6267.

Mazza, F. (2019), "In-plane-out-of-plane non-linear model of masonry infills in the seismic analysis of RC-framed buildings", *Earthq. Eng. Struct. Dyn.*, **48**(4), 432-453. https://doi.org/10.1002/eqe.3143.

Mi, K.H., Yu, W.H. and Bi, S.G. (2022), "Application of PKPM in water conservancy project frame structure design", *China Water Power Electrif.*, **2022**(3), 25-31+64. https://doi.org/10.16617/j.cnki.11-5543/TK.2022.03.06.

Misir, I.S., Ozcelik, O., Girgin, S.C. and Yucel, U. (2016), "The behavior of infill walls in RC frames under combined bidirectional loading", *J. Earthqu. Eng.*, **20**(4), 559-586. https://doi.org/10.1080/13632469.2015.1104748.

Mohammad, A.F., Khalid, F. and Khan, R.A. (2022), "Finite element micro-modelling of RC frames with variant configurations of infill masonry", *Struct. Eng. Mech.*, **81**(4), 395-409. https://doi.org/10.12989/sem.2022.81.4.395.

Qi, X. and Pantazopoulou, S.J. (1991), "Response of RC frame under lateral loads", *J. Struct. Eng.*, **117**(4), 1167-1188. https://doi.org/10.1061/(ASCE)0733-9445(1991)117:4(1167).

Tan, Q., Wu, B., Shi, P., Xu, G., Wang, Z., Sun, J. and Lehman, D.E. (2021), "Experimental performance of a full-Scale spatial RC frame with buckling-restrained braces subjected to bidirectional loading", *J. Struct. Eng.*, **147**(3), 04020352. https://doi.org/10.1061/(ASCE)ST.1943-541X.0002928.

Tong, Y.S. and Qian, G.F. (1982), "Deformation behavior and bearing capacity of reinforced concrete frame with brick-filled walls", *J. Xi'an Univ. Arch. Technol. (Nat. Sci. Ed.)*, **42**(2), 1-21.

Tong, Y.S. and Qian, G.F. (1982), "Experimental study on behavior of reinforced concrete frame with brick-filled walls under horizontal load", *J. Xi'an Univ. Arch. Technol. (Nat. Sci. Ed.)*, **14**(2), 1-13.

Typhoon Webpage in National Meteorological Centre of China (2023), http://typhoon.nmc.cn/web.html.

Wan, W., Bo, J.S., Li, X.B., *et al.* (2013), "Earthquake damage prediction method for highrise buildings based on PKPM program", *World Earthq. Eng.*, **29**(3), 139-144. https://doi.org/10.3969/j.issn.1007-6069.2013.03.021.

Wang, Z.H. and Wang, M.F. (2016), "Research on damping property of reinforced concrete frame structures", *Earthq. Eng. Eng. Dyn.*, **36**(3), 92-101. https://doi.org/10.13197/j.eeev.2016.03.92.wangzh.012.

Wu, C.B., Wang, J.X., Ji, X.D., Jiang, Q., He, J.J. and Liang, Y.S. (2021), "Spatial and temporal statistical characteristics of air density and its influence on basic wind pressure: A case study of Shandong province, eastern China", *J. Beijing Forestry Univ.*, **43**(5), 99-107. https://doi.org/10.12171/j.1000-1522.20210064.

Wu, H.Q. (2013), "Application of Revit software to PKPM design of energy efficiency for power plant buildings", *Eng. J. Wuhan Univ.*, **46**(S1), 30-33.

Yan, B.W., Huang, L. and Deng, L. (2010), "Approach of the collapses of RC frame structure school buildings", *Earth and Space 2010: Engineering*, *Science*, *Construction*, *and Operations in Challenging Environments*, **2010**, 2653-2662. https://doi.org/10.1061/41096(366)249.

Zhang, Y., Ni, Y.Q., Jia, X. and Wang, Y.W. (2023), "Identification of concrete surface damage based on probabilistic deep learning of images", *Autom. Constr.*, **156**(1), 105141. https://doi.org/10.1016/j.autcon.2023.105141.

PL